CIRP Annals - Manufacturing Technology 00 (2020) 1–4

Contents lists available at ScienceDirect

CIRP Annals - Manufacturing Technology

journal homepage: https://www.editorialmanager.com/CIRP/default.aspx

Compressive behavior of 420 stainless steel after asynchronous laser processing

M.P. Sealy[a,*], H. Hadidi[b], L.D. Sotelo[a], W.L. Li[a], J.A. Turner[a], J.A. McGeough (1)[c]

[a] Department of Mechanical and Materials Engineering, University of Nebraska, Lincoln, NE 68588, United States
[b] Department of Mechanical Engineering, Jazan University, Gizan, Jazan, 45142, Saudi Arabia
[c] School of Engineering, The University of Edinburgh, Edinburgh EH9 3FB, UK

ARTICLE INFO

Article history:
Available online xxx

Keywords:
Additive manufacturing
Surface integrity
Laser peening

ABSTRACT

Cold working layers during additive manufacturing improves toughness by imparting a complex glocal integrity across pre-designed internally reinforced domains. Understanding mechanical behavior by mapping glocal integrity across these domains is difficult due to highly heterogeneous compositions formed by cyclic printing and peening. Ultrasound is proposed as a rapid, non-destructive tool to measure glocal integrity that is sensitive to heterogeneous organization of microstructure and residual stress. This work examines compressive behavior and measures glocal integrity with ultrasonic wave speed and attenuation perpendicular to the build direction after cyclically coupling laser engineered net shaping (LENS®) with laser peening on 420 stainless steel.

1. Introduction

Glocal integrity is a cumulative surface integrity enabled by secondary processing of individual layers during additive manufacturing (AM) [1]. For example, laser peening during 3D printing imparts cold worked regions, also referred to as pre-designed internal reinforced domains [2], which evolve and interact with each other as a build progresses. Understanding the resulting glocal integrity from integrating surface treatments on predefined layers is important for improving part quality and performance. Thus, the objective of this study was to understand how asynchronously coupling laser peening with LENS® affected compressive behavior of 420 stainless steel by mapping the resulting glocal integrity using bulk wave ultrasound.

AM quality control has relied on process parameter optimization and continuous process monitoring to advance industry adoption by mitigating defect formation (*e.g.*, cracks, pores, or warpage) and correcting detected defects [3,4]. A complementary strategy to improve quality and performance independent of the AM process or monitoring technology is imparting a complex, predesigned glocal integrity with interlayer surface treatments [5]. While tools for quantitatively measuring surface integrity are well-established [6], these techniques are inefficient and/or impractical for measuring glocal integrity. Extending surface characterization techniques to measure glocal integrity is problematic because of the high resolution required throughout a relatively large build volume. As a result, there is a need for efficient, non-destructive approaches to map glocal integrity of internal reinforced domains that would enable new design paradigms for manufacturing. The following section discusses limitations of current techniques to map glocal integrity and proposes an alternative, non-destructive method more readily adoptable by industry.

1.1. Methods to evaluate glocal integrity

The most common surface integrity metrics mapped below surfaces in AM include microstructure, hardness, and residual stress [1,7,8]. Some measurement techniques are nondestructive, while others require cutting or material removal capable of altering the original surface integrity. Apart from unintended modifications, the challenge in characterizing glocal integrity on cross-sectioned surfaces is how to achieve high resolution mapping efficiently across relatively large surface areas. Typical depths for surface integrity mapping using techniques such as electron microscopy, diffraction, or indentation are 100′s of microns to several millimeters; however, high-resolution maps across several centimeters are necessary to capture changes to glocal integrity from interlayer cold working. Other destructive techniques that use relaxation to capture elastic deformation from cutting or removing material (*e.g.*, hole drilling, slitting, and the contour method for residual stress) have either limited penetration depths and resolution or place constraints on geometry, size, or cut quality [9].

Non-destructive methods to evaluate glocal integrity include diffraction, spectroscopy, magnetization, and acoustics. Diffraction-based methods, such as XRD or EBSD, are commonly used to assess residual stress and microstructure; however, penetration depths are limited without layer removal to less than 10 microns using depth resolved scattering vector residual stress measurements [10]. Other diffraction-based methods include synchrotron *x*-rays and neutrons. While penetration depths increase to several centimeters, access to a major scientific facility is required [9]. Further, neutron diffraction is non-destructive; however, samples can become radioactive for several years.

Raman spectroscopy is a non-destructive surface analysis method based on scattering photons and is capable of analyzing chemical composition, microstructure, and stress [6]. Magnetic methods (*i.e.*, Barkhausen noise) to assess stress and microstructure have slightly higher penetration depths than Raman spectroscopy or x-

* Corresponding author.
E-mail address: sealy@unl.edu (M.P. Sealy).

https://doi.org/10.1016/j.cirp.2020.04.059
0007-8506/

Table 1
Mechanical behavior from interlayer cold working during additive manufacturing.

AM Process	Surface Treatment	Material	Total treated layers	Layer treatment frequency	Gage length (mm)	Gage thick. (mm)	Gage width (mm)	Approximate number of treated layers in gage section (layers)	Notes	Ref.
1. Powder bed fusion	ultrasonic peening	316 SS	6 plus surface	16	25	2	6	7	Increased tensile strength approximately 37% while ductility decreased more than 60% over an as-printed sample	[12]
2. Wire+arc	rolling	Ti-6Al-4V	20	1 (every layer)	27	4	6	4–5 1–2	Ductility remained relatively unaffected; however, anisotropic behavior was eliminated and attributed to finer equiaxed prior β grains from interlayer rolling	[13]
3. Wire+arc	rolling	Al alloys (2219 & 2024)	44–76	1 (every layer)	38.3	2.5	10	20–30 5–8	Improved strength approx. 90% and reduced ductility nearly 50%. Post-build heat treatment had a greater effect than interlayer rolling	[13, 14]
4. Powder bed fusion	ultrasonic peening	316 SS	6 plus surface	16	100	2	10	7	18% increase in buckling strength; no delamination observed	[12]

rays (*i.e.*, several microns to millimeters [9,11]), but are predominately used for surface analysis due to trade-offs between resolution and accuracy with increasing depth. Further, magnetic methods are limited to ferromagnetic materials. Acoustic methods include acoustic microscopy, acoustic emissions, and ultrasonics [6]. Acoustic microscopy has a limited penetration depth of a few millimeters. Although acoustic emissions are capable of volumetric mapping, an external stimulus is required for active listening of released energy. An alternative approach capable of penetrating several centimeters is ultrasonics.

1.2. Influence of glocal integrity on strength

The effect of interlayer cold working on mechanical behavior is poorly understood. New process parameters to consider include layer treatment frequency, total number of treated layers, and load orientation with respect to treated layers. Other critical factors affecting mechanical behavior include the penetration depth of the secondary cold working process and the heat energy from printing on a previously treated layer. The heat from subsequent printing can remove beneficial effects due to thermal cancelation [15].

Interlayer rolling on Al-alloys printed with wire+arc AM (WAAM) [14] and ultrasonic peening on 316 stainless steel printed by powder bed fusion [12] demonstrated improved strength at a cost of reduced ductility (Table 1). However, different alloys subjected to the same hybrid treatment do not always exhibit the same behavior. For example, the ductility of Ti-6Al-4 V remained relatively unaffected by interlayer rolling during WAAM. More studies are needed to understand the resulting mechanical behavior as well as the interdependence on glocal integrity. Thus, the objectives of this study were to measure the compressive properties and map the resulting glocal integrity from coupling laser peening with LENS® using ultrasonics.

2. Asynchronous laser printing and peening

Micro-Melt 420 stainless steel powder (Carpenter Powder Products, USA) was asynchronously printed and laser peened (LP) based on the procedure described in [1]. Cylinders of 12.7 mm diameter and 25.4 mm height were printed on an Optomec LENS® HY20-CA directed energy deposition system. Approximately 17 out of 85 layers were peened. An estimated 2 to 3 peened layers were machined away while cutting off the build plate and squaring parallel faces for ultrasound measurements. The LP power density was 12.7 GW/cm^2. LP overlap was 50% and was repeated five times. The layer treatment frequency was every five layers (L5).

3. Quasi-static compression testing of 420 stainless steel

Quasi-static compression tests of hybrid, as-printed, and wrought 420 stainless steel samples were conducted on a Southwark Emery load frame calibrated by Instron and equipped with a 3 ton load cell. Load data were collected from the load frame using a linear variable differential transformer (LVDT) sensor. The full field deformation was captured using ARAMIS digital image correlation (DIC) as shown in Fig. 1. The 25.4 mm long compression samples were cut in half by wire-EDM to achieve an aspect ratio of approximately 1:1. The terminology "bottom" indicates samples closest to the build plate. Each experiment was repeated twice. Tests were conducted at room temperature (25 °C) with a displacement rate of 0.014 mm/s corresponding to a strain rate of 10^{-3} s^{-1}.

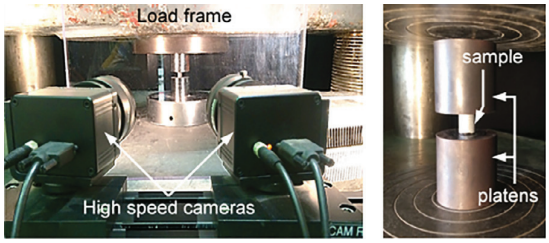

Fig. 1. Compression test of 420SS whereby strain was measured using ARAMIS digital image correlation. (For interpretation of the references to colour in this figure legend, the reader is referred to the web version of this article.)

The as-printed (LENS®) and hybrid-L5 sample showed a significant increase in yield strength compared to wrought 420 SS (Fig. 2). As expected, the as-printed sample exhibited the lowest strain to failure. Introducing interlayer laser peening during LENS® increased the maximum strain to failure more than 50% compared to as-printed samples. As a result, interlayer peening increased the toughness of 420SS over the wrought or as-printed samples. Mechanical properties are provided in Table 2.

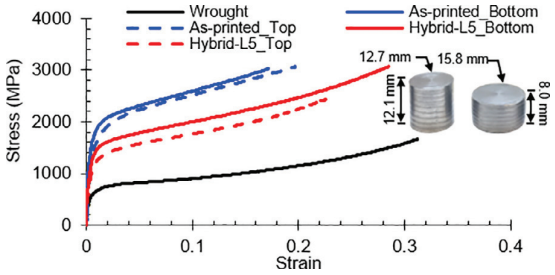

Fig. 2. Stress-strain response for wrought, as-printed (LENS®), and hybrid-L5 (LENS® +LP) 420SS under quasi-static compression (10^{-3} s^{-1}).

Table 2
Mechanical properties of 420SS from uniaxial compression test.

Mechanical properties	Wrought (*n* = 4)	As-printed (LENS) (*n* = 2)	Hybrid L5 (LENS® + LP) (*n* = 2)
Yield strength (MPa)	626 ± 14	1687 ± 15 (T) 1888 ± 88 (B)	1233 ± 18 (T) 1450 ± 30 (B)
Max. strain to failure (%)	31.1 ± 0.1	16.2 ± 1.2 (T) 18.4 ± 1.2 (B)	25.6 ± 2.7 (T) 28.4 ± 0.1 (B)
Toughness (MPa)	334 ± 1	398 ± 6 (T) 440 ± 20 (B)	429 ± 2 (T) 619 ± 1 (B)

Note: (T) indicates top, and (B) indicates bottom; sample size (n).

Please cite this article as: M.P. Sealy et al., Compressive behavior of 420 stainless steel after asynchronous laser processing, CIRP Annals - Manufacturing Technology (2020), https://doi.org/10.1016/j.cirp.2020.04.059

Interestingly, the max strain to failure varied between the top and bottom hybrid samples although the results for the as-printed sample were more uniform. This difference in behavior is thought to be the result of variations in mechanical properties, microstructure, and residual stresses present within the samples. Ultrasonic methods are nondestructive and have been used to quantify elastic properties and grain size. In addition, ultrasound phase velocities have been correlated with residual stress. For this reason, volumetric mapping with ultrasound is examined with respect to the observed mechanical behavior of these samples.

4. Volumetric mapping of glocal integrity by ultrasound

Linear bulk wave ultrasound was used to measure longitudinal wave speed and attenuation in 420 stainless steel samples after coupling LENS® and laser peening. Parallel faces were ground on each sample in both the axial and lateral directions to provide a uniform surface for ultrasound. Ultrasound signals were collected in a pulse–echo measurement configuration using a spherically focused broadband immersion transducer (15 MHz; 76.2 mm focal length in water). A pulser/receiver (DPR 300 from JSR Ultrasonics, Pittsford, NY) using a 64–bit, 2 GHz digital signal processing were used to pulse, receive, and digitize the signals. A personal computer operating UTWin software (Mistras, Schoolcraft, MI) was used to control the data acquisition and the motion of the transducer. Low gain signals were collected to quantify the wave speed using a cross correlation approach and attenuation was calculated by comparing multiple backwall echoes in the frequency domain and by employing a diffraction correction using measurements from fused silica. The focus was placed near the middle of each sample such that the front and back walls were clearly visible and unsaturated. The minimum scanned area was 4 mm by 20 mm with a step size of 0.25 mm (*i.e.*, at least 1600 waveforms per scan). For completeness, more details on the experimental methods and results are available in [16].

4.1. Wave speed correlates with residual stress

One of the goals of this research is to quantify the residual stress using measured wave speed. The speed of elastic waves traveling within a material is known to be affected by the presence of residual stress. Previous researchers have shown the relationship between stress and velocity through acoustoelastic constants [9]. However, there are three major challenges for the quantification of residual stress with ultrasound. First, many models assume a uniaxial stress state, which is unlikely to be present in AM or hybrid-AM samples. Second, the acoustoelastic constants are difficult to obtain and may vary throughout the build. Lastly, the inversion for stress requires knowledge of the baseline velocity for the unstressed material. The velocity is affected to a major extent by the material texture that is usually present in AM samples. Ultrasonic scattering measurements may help us quantify the texture, but that work is beyond the scope of this article.

Trends of residual stress can be observed by examining variations in wave speed across the sample. The measured wave speeds were normalized by the wave speed measured in the wrought sample (6.0640 ± 0.0026 mm/μs). The resulting maps of the normalized wave speed are shown in Fig. 3 for the as-printed and hybrid samples. In the as-printed sample, the wave speed ratio increased monotonically from the top to the bottom (*i.e.*, base plate), and remains less than one for the entire sample. The hybrid sample shows a local maximum 2 mm to 4 mm from the top of the sample and then a decrease towards the bottom. These results suggest that the differences in compressive strength can be attributed to residual stress – lower wave speeds appear to correlate with higher compressive strength.

The wave speed ratios were averaged across the lateral direction so that the variation in the build direction can be examined with respect to the corresponding microhardness data from [1]. These results are shown in Fig. 4. Two observations can be made. First, the global trend of microhardness over the length of the hybrid sample is tracked by the wave speed. In addition, the local variations are also tracked, although the beam width of 700 μm limits the resolution of the ultrasound mapping.

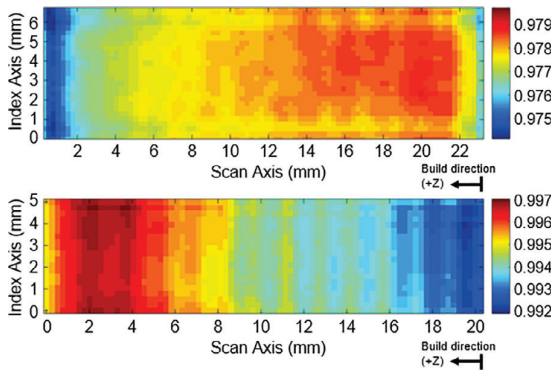

Fig. 3. Measured wave speed ratio maps. Note the differences in scale. (For interpretation of the references to colour in this figure legend, the reader is referred to the web version of this article.)

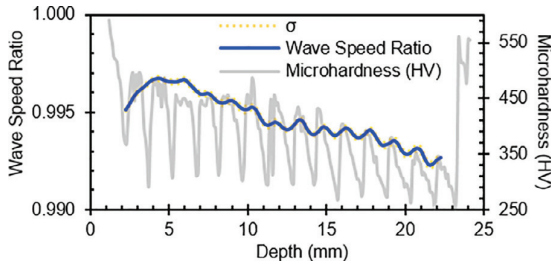

Fig. 4. Wave speed ratio and standard deviation σ in relation to microhardness in hybrid-L5 420SS. Microhardness data obtained from [1].

4.2. Attenuation correlates with grain size

The longitudinal attenuation maps from the as-printed and hybrid samples can be used to identify variations in microstructure across the samples. For wavelengths that are much longer than the grain size, the attenuation is known to scale with the grain volume. Residual stress also affects attenuation, but it is a secondary effect. Therefore, the results from the AM samples can be scaled according to the grain size from the wrought sample. In other words, the cube root of the attenuation ratio should be proportional to the ratio of the grain diameters. The resulting maps are shown in Fig. 5. Away from the sample edges, the microstructure of the as-printed sample appears to be fairly uniform and slightly larger than that of the wrought sample ($\sim$30 μm). The results for the hybrid sample are more interesting with two key trends. First, the fluctuations in grain size clearly show the effect of the laser peening. The bands near the top of the sample are evenly spaced, but those near the build plate become wider and the grains become larger. These measurements can explain the differences in max strain to failure for these samples. The top and bottom halves of the as-printed sample do not show much difference. However, the hybrid sample shows larger grains in the bottom half of the sample, which explains the increase in max strain to failure for that sample. Larger grains allow for more dislocation motion through the bottom samples.

Please cite this article as: M.P. Sealy et al., Compressive behavior of 420 stainless steel after asynchronous laser processing, CIRP Annals - Manufacturing Technology (2020), https://doi.org/10.1016/j.cirp.2020.04.059

The grain diameter ratio was averaged across the lateral dimension of the hybrid sample and is shown in Fig. 6 in comparison with the microhardness data. The regions with larger grain size correlate well with the reduction in hardness as expected. In addition, the global reduction in hardness close to the base plate is correlated with an increase in grain size.

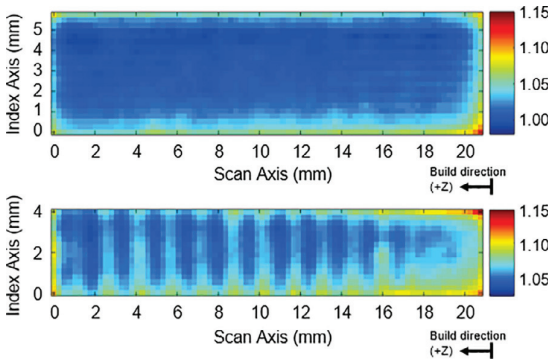

Fig. 5. Grain diameter ratio maps. Note the differences in scale.

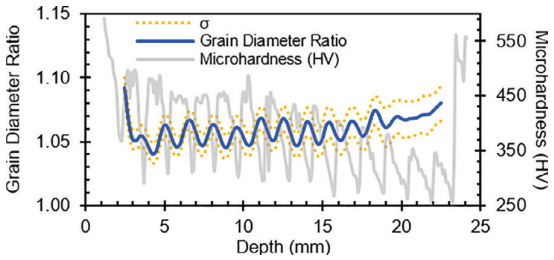

Fig. 6. Grain diameter ratio profile with standard deviation σ in relation to microhardness in hybrid-L5 420SS. Microhardness data provided by [1].

5. Summary and conclusions

This work examined the resulting glocal integrity using bulk wave ultrasound to understand compressive behavior after cyclically coupling laser engineered net shaping (LENS®) with laser peening (LP) on 420 stainless steel. Every fifth layer was peened five times during printing at 50% overlap. Cold working layers during additive manufacturing imparted a complex glocal integrity that was mapped throughout the build volume using ultrasonic wave speed and attenuation along the build direction. Ultrasound was preferred as a rapid, non-destructive tool to map glocal integrity due to its sensitivity to heterogeneous organization and penetration depth for residual stress and microstructure to explain compressive behavior.

The extensive application of LP increased the ability of 420 stainless steel to endure higher deformation and attain a higher toughness. Peening imparted both compressive and tensile residual stresses that were redistributed by highly localized heat from LENS® printing. The normalized wave speed aligned with observations from microhardness suggesting that complex residual stress fields caused hardness to be lower than as-printed samples reported in [1]. Further, wave speed measurements suggested that differences in compressive strength can be attributed to residual stress – lower wave speeds in as-printed and hybrid samples correlated to higher compressive strength.

Compressive samples were cut in half to achieve an aspect ratio near 1:1 for safety during testing. Interestingly, the max strain to failure and failure strength varied between the top and bottom hybrid samples. The variation in compressive behavior can be explained by observations from ultrasonic measurements. Larger grains near the build plate, as measured by attenuation, resulted in a larger failure strain due to continued dislocation motion. The lower wave speed near the baseplate in the hybrid sample correlated with a higher strength than the tops sample.

Future work will focus on refining the use of ultrasound to directly measure glocal integrity, such as residual stress, microhardness, and microstructure. The inversion of wave speed to quantify residual stress is affected to a major extent by the material texture. Texture as well as grain morphology are not yet considered in the models. Ultrasonic scattering measurements may help quantify texture and mechanical behavior in future work.

Acknowledgements

The research was performed in part in the Nebraska Nanoscale Facility: NSF National Nanotechnology Coordinated Infrastructure under award no. ECCS: 1542182, and with support from the Nebraska Research Initiative through the Nano-Engineering Research Core Facility at the Univ. of Nebraska-Lincoln and by NSF CMMI: 1846478. Further, the authors acknowledge financial support of the lead student investigators from Jazan University, Saudi Arabia (Hadidi) and NSF Graduate Research Fellowship (Sotelo). Lastly, the research was facilitated by the Laser Assisted Nano Eng. Lab under the direction of Dr. Yongfeng Lu .

References

[1] Sealy MP, Hadidi H, Kanger CJ, Yan XL, Cui B, McGeough JA (2019) Glocal Integrity in 420 Stainless Steel by Asynchronous Laser Processing. *CIRP Annals - Manufacturing Technology* 68(1):189–192.
[2] Meyer D, Wielki N (2019) Internal Reinforced Domains by Intermediate Deep Rolling in Additive Manufacturing. *CIRP Annals - Manufacturing Technology* 68 (1):579–582.
[3] Schmidt M, Merklein M, Bourell D, Dimitrov D, Hausotte T, Wegener K, Overmeyer L, Vollertsen F, Levy G (2017) Laser Based Additive Manufacturing in Industry and Academia. *CIRP Annals - Manufacturing Technology* 66(2):561–583.
[4] Everton SK, Hirsch M, Stravroulakis P, Leach RK, Clare AT (2016) Review of In-situ Process Monitoring and In-situ Metrology for Metal Additive Manufacturing. *Mater Des* 95:431–445.
[5] Sealy MP, Madireddy G, Williams R, Rao P, Toursangsaraki M (2018) Hybrid Processes in Additive Manufacturing. *Journal of Manufacturing Science and Engineering* 140(6):1–13. pp. 060801.
[6] Jawahir IS, Brinksmeier E, M'Saoubi R, Aspinwall DK, Outeiro JC, Meyer D, Umbrello D, Jayal AD (2011) Surface Integrity in Material Removal Processes: recent Advances. *CIRP Annals - Manufacturing Technology* 60(2):603–626.
[7] Brinksmeier E, Levy G, Meyer D, Spierings AB (2010) Surface Integrity of Selective-laser-melted Components. *CIRP Annals* 59(1):601–606.
[8] Li C, Liu ZY, Fang XY, Guo YB (2018) Residual Stress in Metal Additive Manufacturing. *Procedia CIRP* 71:348–353.
[9] Schajer GS (2013) *Practical Residual Stress Measurement Methods*, John Wiley & Sons, Ltd.West Sussex, UK.
[10] Breidenstein B, Denkena B, Vetter J, Richter B (2016) Influence of the Residual Stress State of Coatings on the Wear Behavior in External Turning of AISI 4140 and Ti−6Al−4 V. *Production Engineering* 10:147–155.
[11] Sridharan U, Bedekar V, Kolarits FM (2017) A Functional Approach to Integrating Grinding Temperature Modeling and Barkhausen Noise Analysis for Prediction of Surface Integrity in Bearing Steels. *CIRP Annals - Manufacturing Technology* 66(1):333–336.
[12] Gale J, Achuhan A (2017) Application of Ultrasonic Peening during DMLS Production of 316 L Stainless Steel and Its Effect on Material Behavior. *Rapid Prototyp J* 23(6):1185–1194.
[13] Colegrove PA, Donoghue J, Martina F, Gu J, Prangnell P, Hönnige J (2017) Application of Bulk Deformation Methods for Microstructural and Material Property Improvement and Residual Stress and Distortion Control in Additively Manufactured Components. *Scr Mater* 135(Supplement C):111–118.
[14] Gu J, Ding J, Williams SW, Gu H, Bai J, Zhai Y, Ma P (2016) The Strengthening Effect of Inter-layer Cold Working and Post-deposition Heat Treatment on the Additively Manufactured Al−6.3Cu alloy. *Materials Science and Engineering: A* 651: 18–26.
[15] Madireddy G, Li C, Liu J, Sealy MP (2019) Modeling Thermal and Mechanical Cancellation of Residual Stress from Hybrid Additive Manufacturing by Laser Peening. *Nanotechnology and Precision Engineering* 2(2):49–60.
[16] Sotelo LD, Hadidi H, Pratt C, Sealy MP, Turner JA (2020) Ultrasonic Mapping of Hybrid Additively Manufactured Materials. *Ultrasonics* (accepted).